The Astrophysical Journal, 678:549–562, 2008 May 1

SUPERNOVA COLLISIONS WITH THE HELIOSPHERE

Brian D. Fields, Themis Athanassiadou, and Scott R. Johnson
Center for Theoretical Astrophysics, Departments of Astronomy and Physics, University of Illinois, Urbana, IL 61801; bdfields@uiuc.edu, athanssd@uiuc.edu, srjohns1@uiuc.edu
Received 2006 November 22; accepted 2007 September 5

ABSTRACT

Nearby supernova explosions—within a few tens of pc of the solar system—have become a subject of intense scrutiny, due to the discovery of live undersea ^{60}Fe from an event 2.8 Myr ago. A key open question concerns the delivery of supernova ejecta to the Earth, in particular penetration of the heliosphere by the supernova remnant (SNR). We present the first systematic numerical hydrodynamical study of the interaction between a supernova blast and the solar wind. Our simulations explore dynamic pressure regimes that are factors $\geq$10 above those in other studies of the heliosphere under exotic conditions, for supernovae exploding at a range of distances through different interstellar environments, and interacting with solar winds of varying strengths. Our results are qualitatively consistent with the structure of the contemporary heliosphere modeled by previous work, but compressed to within the inner solar system. We demonstrate that key characteristics of the resulting heliospheric structure follow simple scaling laws that can be understood in terms of pressure-balance arguments, and which are in agreement with previous work. Our models show that a 10 pc supernova event, incident on a solar-wind outflow with the mean observed properties, compresses the heliopause to just beyond 1 AU. We also demonstrate scenarios where the supernova remnant compresses the heliopause to within 1 AU, in which cases supernova material will be directly deposited on Earth. Since 8 pc marks the nominal "kill radius" for severe biosphere damage, any extinction-level events should have left terrestrial deposits of supernova debris. We conclude with a brief discussion of the effect of our approximations and the impact of additional physics.

Subject headings: astrobiology — interplanetary medium — solar wind — supernovae: general

Online material: color figures

1. INTRODUCTION

The consequences and signatures of supernova explosions near the solar system (or other planetary systems) have been the subject of speculation for almost a half century (Schindewolf 1954; Krasovskii & Shklovskii 1957; Terry & Tucker 1968; Laster et al. 1968; Benítez et al. 2002). The topic is rich, spanning astrophysics, geoscience, and now astrobiology. Special attention has been focused on the effect of a nearby supernova on the terrestrial environment. Ruderman (1974) showed the primary effect to be damage to, or outright removal of, ozone in the upper atmosphere (e.g., Ruderman 1974; Crutzen & Brühl 1996; Gehrels et al. 2003), although other effects have been considered (e.g., Fields & Ellis 1999). This in turn could lead (Karam 2002a, 2002b) to a significant insult to the biosphere and/or stimulation of beneficial genetic variation. On the basis of these effects, the "minimum safe distance" from a supernova is estimated at $\sim$8 pc (Ellis & Schramm 1995; Gehrels et al. 2003).

Our understanding of the astrophysics and astrobiology of nearby supernovae can only move beyond speculation in the presence of a concrete empirical signature of such an event. Ellis et al. (1996) showed in detail how such a signature can be obtained by the detection of live radioisotopes with lifetimes shorter than the age of the solar system. These species lack a strong terrestrial background, a crucial advantage in the face of the tiny expected supernova signal. Knie et al. (1999) first reported detection of such live radioactivity, in the form of accelerator mass spectrometry measurements of ^{60}Fe($t_{1/2} = 1.5$ Myr) in a deep-ocean ferromanganese crust. The ^{60}Fe abundance, while tiny, exceeds known backgrounds by a factor of $\sim$100, and thus can only be understood as a supernova signature (Knie et al. 1999; Fields & Ellis 1999). Recently, Knie et al. (2004) confirmed this detection by identifying ^{60}Fe in another crust with much better time resolution, which pinned down the supernova epoch to 2.8 ± 0.4 Myr ago. This landmark discovery opens the way for "supernova archeology." For example, the ^{60}Fe abundance yields a supernova distance of 15–100 pc, where the large uncertainty is dominated by large variations in the supernova ^{60}Fe yield (Fields et al. 2005). The upper end of the distance range is consistent with the location of the Scorpius-Centarus OB association (the nearest site of massive star formation) at the time of the explosion (Benítez et al. 2002). Such a nearby and relatively recent event may play a role in forming and/or sustaining the hot, rarefied Local Bubble in which the Sun is currently embedded (Smith & Cox 2001).[1]

A physically clear and quantitatively accurate understanding of the penetration of a supernova blast into the heliosphere is critical for understanding both the impact of a nearby supernova on the biosphere and the deposition of observable radioisotopic supernova signatures. Currently, however, no detailed models exist that directly and systematically address this problem. Ellis et al. (1996) briefly addressed supernova collisions, but this was limited to a

[1] Since this paper was initially submitted, Basu et al. (2007) have detected large abundances of ^{3}He in the same crust; this isotope is also found in sea sediments, and is likely due to the infall of cosmic ray–irradiated dust. This result confirms that extraterrestrial material can indeed become incorporated into these crusts. ^{3}He abundances in the crust show a significant increase over the past $\sim$4 Myr, although a correlation with the ^{60}Fe spike is not seen. Basu et al. (2007) argue that because the ^{3}He can be understood as having a solar system origin, it is possible that the ^{60}Fe might have been delivered in one or a few very large ($\gtrsim$0.5 mm) iron/nickel-rich micrometeorites. On the other hand, if the ^{60}Fe is of meteoritic origin, it should be accompanied by a similarly large spike in ^{53}Mn, which has not been found for this crust. A detailed study of this issue is warranted, but goes beyond the scope of this paper; in any case, the motivation for and importance of nearby supernova studies goes beyond the ^{60}Fe evidence.

simple order-of-magnitude estimate, which used a momentum-conservation argument to infer a maximum penetration distance on the order of a few tens of pc. After decades of effort (Axford et al. 1963; Patterson et al. 1963), extensive analytical and numerical studies of the present heliosphere do exist and provide a useful theoretical and numerical framework (e.g., Zank 1999; Baranov 1990 and references therein). While the present heliospheric conditions are very different (with collision speeds an order of magnitude smaller) from those in a supernova impact, two studies in particular have simulated the heliosphere in a wide variety of interstellar environments (Zank & Frisch 1999; Müller et al. 2006). These come the closest to our own work, offering invaluable insights and points of quantitative comparison; our study follows the approach and analytical techniques laid out in these papers. Even these simulations, however, consider parameters considerably less extreme than those produced by a supernova: the fastest interstellar velocities in Müller et al. (2006) have ram pressures an order of magnitude smaller than those we will consider, and the heliopause standoff never comes closer than tens of AU.

To date, no gas dynamics calculation has self-consistently addressed the supernova evolution and blast passage together; also, no study has systematically addressed the detailed structure and dynamics of the collision with the heliosphere for a range of supernova parameters. This paper represents a first step toward filling this gap in our knowledge. We present the first gas dynamics simulations to make a detailed, systematic study of supernova remnant collisions with the heliosphere. Our work is based on FLASH (Fryxell et al. 2000), an adaptive mesh code which is adept at shock capturing, and is thus well suited for our problem. Our study is in two parts. We first construct simple models of supernova remnant evolution, and from this derive the properties of the remnant fluid over its history as it passes observers at different distances. The important point here is that the supernova remnant is large compared to 1 AU, and that its passage is very long lived ($\gtrsim$1 kyr) compared to characteristic timescales for solar wind response ($\sim 1\ \mathrm{AU}/v_{\mathrm{sw}} \sim 1$ day). Consequently, on the length and time scales of the heliosphere collision problem, we may treat the supernova blast as a uniform wind, whose properties we derive from our remnant simulation.

We then zoom into scales of a few AU and perform simulations of the collision of a supernova with the solar wind. Our numerical work is guided and checked against analytical results, some of which have been derived for the case of the present heliosphere (e.g., Baranov 1990). Numerical simulations of the heliosphere under present-day (e.g., Zank 1999 and references therein) and exotic conditions (Müller et al. 2006) similarly provide invaluable qualitative insight and quantitative benchmarks. We find that the basic structure of the supernova–solar wind collision is quite similar to that of the present-day heliosphere, whose terminology we borrow. Since both flows are initially supersonic, there are two shocks: a termination shock marking the deceleration of the solar wind, and a bow shock in the supernova flow. A contact discontinuity, the heliopause, forms at the interface of the supernova and solar wind flows. The heliopause is of particular interest for our problem, as it marks the innermost boundary of supernova material. We find that the heliopause is subject to Kelvin-Helmholtz instabilities, the presence of which smears out somewhat the region of "supernova contamination" beyond the values obtained from simple pressure-balance estimates of distance of closest approach (stagnation point).

Our results depend on various physical parameters, particularly the supernova distance, as well as the strength of the solar wind (i.e., phase in the solar cycle) and the density of the interstellar medium into which the supernova explodes. We examine the effect of these parameters, and find that the supernova distance is the most important; for the heliopause to penetrate to within 1 AU, we find that a supernova distance not much more than 10 pc is required. However, we find that some of these dependencies are linked by scaling relations, which we derive and test. These scalings not only allow for useful semi-analytical treatment of the supernova collision problem, but also allow a comparison with the very similar relations found in models of the heliosphere in a wide variety of other environments (Müller et al. 2006). Our results extend these to extreme impact velocities.

2. OBSERVATIONAL DATA

2.1. *The Solar Wind*

The solar wind is a time-varying, non-axisymmetric, multicomponent, magnetohydrodynamic flow; a full description of the solar wind should include these properties. However, for our initial investigations we will adopt an idealized model of the solar wind, with attention to reproducing the bulk properties at 1 AU and globally. Here, we will summarize these properties, some of which will be inputs to our simplified description, and some of which will be checks on it.

At 1 AU, the observed properties of the solar wind plasma vary with time, particularly over the solar cycle, but also on shorter timescales. For a period roughly spanning the calendar year 1996, the *Solar and Heliospheric Observatory* (*SOHO*) found (Ipavich et al. 1998) a proton number density $n_{p,\mathrm{sw}} = 8.1 \pm 4.3\ \mathrm{cm}^{-3}$ and speed $v_{\mathrm{sw}} = 421 \pm 76\ \mathrm{km\ s}^{-1}$, where in both cases the first value gives the time-averaged mean, and the error range indicates the variance, which is much larger than the measurement error. Furthermore, Ipavich et al. (1998) found that the solar wind density and velocity are anticorrelated, with a best-fit power-law relation $n_{p,\mathrm{sw}} = 7.6\ \mathrm{cm}^{-3}(v_{\mathrm{sw}}/400\ \mathrm{km\ s}^{-1})^{-1.92}$. Thus we see that the solar wind ram pressure,

$$P_{\mathrm{ram,sw}} = m_p n_{p,\mathrm{sw}} v_{\mathrm{sw}}^2 \approx 2.0 \times 10^{-8}\ \mathrm{dyne\ cm}^{-2}, \qquad (1)$$

is nearly independent of the solar wind speed, with a very weak scaling as $P_{\mathrm{ram,sw}} \propto (v_{\mathrm{sw}}/400\ \mathrm{km\ s}^{-1})^{0.08}$.

This finding that the solar wind ram pressure is roughly constant over a solar cycle is fortuitous for our problem, since we will soon see that force (i.e., pressure) balance sets the maximum penetration of the supernova remnant. The constancy of solar wind ram pressure has been noted in previous studies (Steinitz & Eyni 1980; Mullan 1983; Leinert & Jackson 1998) that span larger ranges over the solar cycle.

Still, while the ram pressure variance is less than it would be if the density and speeds were uncorrelated, it is still large; Ipavich et al. (1998) find $P_{\mathrm{sw,ram}} = (2.2 \pm 0.9) \times 10^{-8}\ \mathrm{dyne\ cm}^{-2}$. The large excursions $\Delta P_{\mathrm{ram}}/P_{\mathrm{ram}} \sim \vartheta(1)$ imply for our problem that we can expect that the supernova penetration will in general fluctuate significantly over a single solar cycle, in addition to long-term secular variations due to the supernova blast profile and/or solar variations. Furthermore, it is worth noting that much of the analysis has been on data taken near the ecliptic plane. In traversing from one heliocentric pole to another, *Ulysses* found that the solar wind ram pressure was stronger toward the poles. Phillips et al. (1995) reported $P_{\mathrm{ram,poles}} \simeq 3 \times 10^{-8}\ \mathrm{dyne\ cm}^{-2}$ (scaled to 1 AU), which is roughly a 50% enhancement above the mean equatorial value. Thus in our collision problem, one might imagine that the maximum penetration distance might well depend on the inclination of the ecliptic relative to the incoming supernova blast.

In light of these trends, our approach in the present study will be to focus on the heliospheric collision response for typical solar

TABLE 1
Adopted Interstellar Medium Parameters for Supernova Simulations

ISM Model	Density, n_H (cm^{-3})	Temperature, T (K)	Pressure, P (dyne cm^{-2})
Local Interstellar Cloud.....	0.1	8000	2.2×10^{-13}
Local Bubble.....	0.005	1.28×10^{6}	1.8×10^{-12}
Average ISM.....	1.0	8000	2.2×10^{-12}

wind parameters. We will adopt fiducial solar wind parameters such that the (unperturbed) density and velocity values at 1 AU are near (within $\simeq$10%) the means reported by Ipavich et al. (1998). We will take particular care that our fiducial ram pressure $P_{sw,ram} = 2\times10^{-8}$ dyne cm^{-2}. We will also explore the response of different ram pressures, but will defer a thorough study of these variations to forthcoming work.

2.2. *The Local Interstellar Medium*

The present-day structure of the local interstellar medium (LISM) and of the heliosphere both provide qualitative insight, as well as quantitative inputs for the nearby supernova problem.

The nature of the LISM today sheds light on the ambient conditions one might expect for a recent nearby supernova.[2] The present ISM in the $\sim$100 pc region surrounding the heliosphere consists of a hot, low-density gas. This region is thus known as the "Local Bubble" (e.g., Frisch 1995 and references therein). Smith & Cox (2001) suggest that the LISM, particularly its X-ray emission properties, can be understood as a result of multiple supernova explosions, and intriguingly conclude that the most recent event should have been within the past few Myr. In any case, given that the Local Bubble is large enough to exceed the size of a typical supernova remnant, it is likely that an event producing the ^{60}Fe signal 2.8 Myr ago occurred within a pre-existing bubble. At present, the immediate environment of the Sun is the Local Interstellar Cloud (or "local fluff"; Frisch 1995), a relatively small region both denser and cooler than the Local Bubble. The Sun entered this region in the past 10,000 yr, and so at the time of the ^{60}Fe event, the Sun was probably inside the Local Bubble itself.

To study the effect of the presupernova medium, we will examine conditions like that of the Local Bubble, as well as the Local Interstellar Cloud. For comparison, we will also discuss results in which an explosion occurs within a "typical" ISM region, with parameters set at Galactic average values; we will see that the high-density (and high-pressure) values allow for a more distant supernova to drop out of the Sedov phase and into the radiative phase. These sets of ISM parameters appear in Table 1.

2.3. *The Heliosphere*

The present heliosphere has the basic structure defined by the interaction between the solar wind and the LISM through which we move at $v_\odot \sim 26$ km s^{-1}. Zank (1999) provides an excellent review of the solar wind–LISM interaction. The deceleration of the solar wind leads to a "termination shock," where the flow becomes subsonic; the interface between the flows is a contact discontinuity, the "heliopause." If the LISM sound speed is such that $c_s < v_\odot$, then our motion through it is supersonic, leading to a second shock, the "bow shock" which decelerates the interstellar material. The detailed structure and stability of these boundaries, and their distances at closest approach, remains a subject of intense interest.

Recent *Voyager 1* data have enriched (and complicated!) our understanding of the heliosphere. In late 2004, *Voyager 1* experienced a sharp enhancement in magnetic field strength (Burlaga et al. 2005), along with a rise in pick-up ion intensity (Stone et al. 2005) and a steady increase in low-energy cosmic rays (Stone et al. 2005). All of these enhancements have been sustained since, and point to *Voyager 1* having crossed the termination shock at a distance of 94 AU. The termination shock location should vary with the solar cycle, and thus increases in the solar wind ram pressure over 2002–2005 could explain (e.g., Webber 2005) particle enhancements (Krimigis et al. 2003; McDonald et al. 2003) around 85 AU as precursor encounters with a receding heliosheath.

3. ANALYTIC EXPECTATIONS

Some idealized analytical considerations help to elucidate some of the basic scales and structures in our problem; many of these considerations are elucidated for the case of the present-day heliosphere by Baranov (1990) and Zank (1999).

3.1. *Supernova Remnant: Sedov-Taylor Model*

We first consider the largest scales relevant to our problem, set by the development of the supernova blast wave and the SNR. In both our analytical and numerical results, we will take the supernova, the surrounding pre-explosion interstellar medium, and the Sun to all be at rest relative to one another.

For a simple analytic description of the supernova blast, we adopt the spherically symmetric, adiabatic Sedov-Taylor solution (e.g., Landau & Lifshitz 1987). In this model, the supernova shock front position is $R_{SN} = \beta(E_{SN}/m_p n_{ISM})^{1/5} t^{2/5}$, where E_{SN} is the explosion energy, n_{ISM} is the ambient interstellar (hydrogen) density, and $\beta \sim 1$ is a numerical factor weakly dependent on the adiabatic index γ. Here and throughout the numerical expressions, we use $\gamma = 5/3$, which gives $\beta = 1.1517$. Because our detector (the Earth) is at a fixed distance, we will be interested in the remnant properties as a function of SNR radius; for convenience, we list them here. The shock front arrival time at position R_{SN} is

$$t = \beta^{-5/2}\sqrt{\frac{m_p n_{ISM}}{E_{SN}}}R_{SN}^{5/2} = 4.8\ \mathrm{kyr}\left(\frac{n_{ISM}}{1\ \mathrm{cm}^{-3}}\right)^{1/2}\left(\frac{R_{SN}}{10\ \mathrm{pc}}\right)^{5/2}, \quad (2)$$

where here and throughout we adopt a supernova baryonic energy with the canonical value $E_{SN} = 10^{51}$ erg. The shock front speed is

$$v_{shock} = \frac{2}{5}\frac{R_{SN}}{t} = \frac{2}{5}\beta^{5/2}\sqrt{\frac{E_{SN}}{m_p n_{ISM}}}R_{SN}^{-3/2}. \quad (3)$$

The speed of the material behind the shock (i.e., the speed of shocked material flowing downstream of the shock) is

$$v_{SNR} = \frac{2}{\gamma+1}v_{shock} = \frac{4}{5}\frac{\beta^{5/2}}{\gamma+1}\sqrt{\frac{E_{SN}}{m_p n_{ISM}}}R_{SN}^{-3/2} \quad (4)$$

$$= 610\ \mathrm{km\ s}^{-1}\left(\frac{1\ \mathrm{cm}^{-3}}{n_{ISM}}\right)^{1/2}\left(\frac{10\ \mathrm{pc}}{R_{SN}}\right)^{3/2}, \quad (5)$$

[2] Of course, to describe events in the more distant past, one must consider the effect of different phases in a multicomponent interstellar medium, as well as the fact that supernovae will not occur under random interstellar conditions, but rather will explode in environments which have been "preprocessed" by the presupernova ionizing radiation and possibly winds. See discussion in § 8.

as measured *in the ISM frame*. The sound speed behind the shock is $c_s^2 = 2\gamma(\gamma-1)v_{\rm shock}^2/(\gamma+1)^2$, and so the Mach number behind the shock takes the constant value

$$\mathcal{M}_{\rm SNR} = \sqrt{\frac{2}{\gamma(\gamma-1)}} = \sqrt{\frac{9}{5}} = 1.34; \quad (6)$$

i.e., the postshock flow is mildly supersonic.

The density behind the shock is enhanced over the ambient density by the usual compression

$$\rho_{\rm SNR} = \frac{\gamma+1}{\gamma-1}\rho_{\rm ISM} = 4\rho_{\rm ISM}. \quad (7)$$

The postshock ram pressure in the ISM frame is $P_{\rm SNR,ram} = \rho_{\rm SNR}v_{\rm SNR}^2$, and the thermal pressure is $P_{\rm SNR,therm} = 2\rho_{\rm ISM}v_{\rm shock}^2/(\gamma+1)$. Thus the total pressure is

$$P_{\rm SNR,tot} = P_{\rm SNR,ram} + P_{\rm SNR,therm} = \frac{8\beta^5}{25(\gamma-1)}\frac{E_{\rm SN}}{R_{\rm SN}^3} \quad (8)$$

$$= 3.3\times10^{-8}\ {\rm dyne\ cm^{-2}}\left(\frac{10\ {\rm pc}}{R_{\rm SN}}\right)^3. \quad (9)$$

It is worth noting that, as demanded by self-similarity, the supernova pressure scales as E/R^3 and is *independent* of the density of the ambient medium. We will find that pressure balance is the key factor in determining the distance of closest supernova approach, and thus, as long as the remnant is in the Sedov phase, its effect on the solar system will be largely independent of the nature of the ambient medium.

3.2. *Solar Wind*

For our analytic estimates, we consider a steady state, spherically symmetric, adiabatic flow to describe the solar wind. Under these conditions, the mass flux at radius r is directed radially, with magnitude

$$j_{\rm sw}(R_{\rm sw}) = \rho_{\rm sw}v_{\rm sw} = \frac{\dot{M}}{4\pi R_{\rm sw}^2} = j_{\rm sw}(1\ {\rm AU})\left(\frac{1\ {\rm AU}}{R_{\rm sw}}\right)^2, \quad (10)$$

which immediately follows from mass conservation. For distances $\gtrsim$1 AU, we can to a reasonable approximation ignore the acceleration of the solar wind; momentum conservation then implies a constant velocity, so that the density falls off as $R_{\rm sw}^{-2}$, as does the ram pressure. On the other hand, the thermal pressure drops more sharply as $P \propto \rho^\gamma \propto R_{\rm sw}^{-2\gamma}$, and thus beyond 1 AU becomes even more negligible than at 1 AU. We then have

$$v_{\rm sw} \approx v_{\rm sw,1\ AU} \approx 450\ {\rm km\ s^{-1}}, \quad (11)$$

$$\rho_{\rm sw} \approx \rho_{\rm sw,1\ AU}\left(\frac{1\ {\rm AU}}{R_{\rm sw}}\right)^2, \quad (12)$$

$$P_{\rm tot,sw} = \rho_{\rm sw}v_{\rm sw}^2 + P_{\rm sw} \approx \rho_{\rm sw}v_{\rm sw}^2 \approx 2\times10^{-8}\ {\rm dyne\ cm^{-2}}\left(\frac{1\ {\rm AU}}{R_{\rm sw}}\right)^2. \quad (13)$$

We will henceforward refer to these expressions as the "constant-velocity approximation" for the solar wind.

3.3. *Supernova–Solar Wind Collision*

For the incoming supernova blast, we take a steady state uniform adiabatic planar flow. The assumption of planar symmetry is in part for convenience, but also because current observations of supernova remnants are unable to probe this regime, and thus offer no guidance on the scales and amplitudes of possible density variations.[3] We take the supernova flow direction to be in the z-axis, with initial density $\rho_{\rm SNR}$, pressure $P_{\rm SNR}$, and speed $v_{\rm SNR}$.

The geometry of the supernova–solar wind collision thus has axial symmetry about the z-axis. This symmetry guarantees that the point of closest penetration (the stagnation point) will lie along the z-axis, where the solar wind is oriented to directly oppose the supernova blast. In a steady state, we expect force balance, and hence momentum balance, to be established; this will occur when the total pressures (thermal and ram) in the two flows are equal, which occurs at the pressure-balance or stagnation distance (e.g., Baranov 1990)

$$R_{\rm stag} = \sqrt{\frac{P_{\rm sw} + \rho_{\rm sw}v_{\rm sw}^2}{P_{\rm SNR} + \rho_{\rm SNR}v_{\rm SNR}^2}}\ {\rm AU}, \quad (14)$$

where the solar wind quantities are evaluated at $R_{\rm sw} = 1$ AU. Note that since both the solar wind and supernova are supersonic, their thermal pressure is small compared to their ram pressure. As a check on this expression, we can use it to estimate the present-day stagnation point. For a Local Interstellar Cloud density of $n_{\rm ISM} = 0.1\ {\rm cm^{-3}}$ and a relative speed $v_\odot = 26\ {\rm km\ s^{-1}}$, we find a ram pressure $P_{\rm ram,ISM} \simeq 10^{-12}$ dyne cm^{-2}, and thus $P_{\rm tot,ISM} \approx P_{\rm ram,ISM}$. Substituting this for the SNR pressures in equation (14) gives $R_{\rm stag} \simeq 100$ AU, which is in good agreement with present observations (§ 2.3).

The solar wind at 1 AU is observed to have a total pressure $P_{\rm sw} + \rho_{\rm sw}v_{\rm sw}^2 \simeq 2\times10^{-8}$ dyne cm^{-2} (eq. [13]), a value that is just comparable to that of a SNR at 10 pc (eq. [8]). Because of this numerical coincidence, we can see that the stagnation point for a supernova–solar wind collision will be on the order of $R_{\rm stag} \sim 1$ AU. The stagnation distance sets the characteristic length scale in our problem. Moreover, it marks the location of the contact discontinuity, and thus is the innermost boundary of the heliopause, and hence of supernova gas. Obtaining accurate estimates of this distance of maximum penetration by the supernova remnant is a central goal of this paper. Taken at face value, this estimate suggests a penetration cutoff $R_{\rm stag} \sim 1$ AU for a supernova at $R_{\rm SN} \sim 10$ pc, which coincidentally is just around the "minimum safe distance."

The fact that $R_{\rm stag} \sim 1$ AU has major implications for the supernova-heliospheric collision and its geological and biological impact. Immediately we see that indeed supernova penetration to the Earth's orbit is feasible for nearby events at interesting distances (and frequencies; see, e.g., Shklovskii 1968; Fields 2004). Thus we may indeed hope for radioisotope deposition, and possibly terrestrial environmental damage due to the increased cosmic-ray flux due to anomalous and Galactic cosmic rays accelerated in the two shocks.

On the other hand, the fact that the stagnation distance is, within our simplified treatment, *exactly* at the 1 AU boundary implies that

[3] Obviously, the curvature in a perfectly spherical SNR that is parsecs in size will be totally negligible on AU scales, and so our assumption of a planar SNR flow is self-consistent with our SNR simulations. Of course, real SNRs are aspherical, so the true physical situation might be more complicated.

the ability of the supernova remnant to engulf the Earth depends not only on the supernova distance, but also on a number of other factors. One major issue is the nature of the detailed hydrodynamics, especially the possibility of instabilities. At the stagnation point, the initially supersonic solar and supernova flows are both decelerated to zero speed; this requires not only that each flow develop shocks, but also suggests that a contact discontinuity develops that separates the solar wind from the supernova material. The pressure across this discontinuity is continuous, but the density and tangential velocity are discontinuous. This implies that at the stagnation point, the flows are diverted tangentially away from the symmetry axis; due to their unequal densities and surrounding velocity shear, one expects Kelvin-Helmholtz instabilities to result.

Indeed, simulations of the present-day heliosphere do find instabilities. The detailed study of Florinski et al. (2005) identifies Kelvin-Helmholtz instabilities in four-fluid simulations of the heliopause that include the effects of magnetic fields. Moreover, their multifluid approach can and does find Rayleigh-Taylor instabilities, i.e., where a low-density fluid supports a high-density one, with the role of gravity replaced by the momentum transfer through ion-neutral interactions. Kryukov et al. (2006) find similar results in both two-fluid and four-fluid simulations. Instabilities are found in other colliding flows. The intensive study of colliding winds (e.g., Luo et al. 1990; Stevens et al. 1992) in models of binary massive stars with supersonic mass loss demonstrates the onset of Kelvin-Helmholtz instabilities due to the velocity shear across the discontinuity. Instabilities also appeared in the Velázquez et al. (2003) simulations of a SNR collision with a very fast stellar wind, characteristic of massive O-type stars.

Our own nonmagnetic, purely hydrodynamic simulations are blind to magnetohydrodynamic and/or multifluid effects; thus we do not expect to see Rayleigh-Taylor features, but we can (and will) find Kelvin-Helmholtz rolls, features also seen in heliospheric simulations under present-day conditions (Florinski et al. 2005; Kryukov et al. 2006).

The development of such instabilities can lead to significant time fluctuations in the stagnation point. Such excursions in the supernova boundary could be very important for our problem. Thus, we conclude that the closeness of the stagnation point to the crucial 1 AU boundary demands that we pursue the problem further with a full hydrodynamic treatment. As we will see, Kelvin-Helmholtz instabilities do indeed arise in our problem, and do "smear" the separation between supernova and solar wind material.

Another important diagnostic of our problem is the characteristic timescale in the collision problem. The "crossing time" for (unimpeded) supernova material to traverse the stagnation distance is

$$t_{\rm cross} = \frac{R_{\rm stag}}{v_{\rm SNR}} = 4.3 \text{ days } \left(\frac{R_{\rm stag}}{1 \text{ AU}}\right)\left(\frac{400 \text{ km s}^{-1}}{v_{\rm SNR}}\right). \quad (15)$$

This very short duration has two immediate consequences. First, it is clear that timescales in the collision will be very short compared to the >1 kyr time for the passage of a supernova blast (eq. [2]; see also Fig. 2). Thus we cannot hope to directly model the full duration over which the Earth is exposed. Instead, our collision simulations amount to "snapshots" during this process, and we can deduce the net effect of the supernova by an integration over a time series of blast properties. Second, we see that the characteristic timescale in our problem is small, even compared to the 11 year solar cycle. Thus, rather than averaging solar wind properties over the cycle, a better approach is to examine the collision for solar wind parameters corresponding to different phases in the cycle.

4. NUMERICAL METHODS

To study both the evolution of a supernova remnant in its Sedov-Taylor phase, as well as the supernova–solar wind collision problem, we use the FLASH code (Fryxell et al. 2000), an adaptive mesh, parallel simulation code. The hydrodynamic solver used in FLASH is a directionally split piecewise parabolic method (PPM) solver, originally described by Woodward & Colella (1984). PPM is a second-order scheme both in space and time, and performs very well in resolving discontinuities. FLASH uses the PARAMESH library to manage a block-structured grid, placing resolution elements where they are needed most.

Both the PPM solver and the adaptive mesh feature are well suited for our problem, in which we encounter shocks and contact discontinuities, as well as hydrodynamic instabilities that can be resolved without too much computational expense.

We employ FLASH to solve the Euler equations of hydrodynamics with a cooling source term. These can be written as:

$$\frac{\partial \rho}{\partial t} + \nabla \cdot (\rho \boldsymbol{v}) = 0, \quad (16)$$

$$\frac{\partial \rho \boldsymbol{v}}{\partial t} + \nabla \cdot (\rho \boldsymbol{v}\boldsymbol{v}) + \nabla P = 0, \quad (17)$$

$$\frac{\partial (\rho E)}{\partial t} + \nabla \cdot [(\rho E + P)\boldsymbol{v}] = -\Lambda(T) n^2, \quad (18)$$

where ρ is the mass density of the fluid, n_p is the proton (and electron) number density, $\boldsymbol{v}$ its velocity, P is the thermal pressure, and E is the total specific energy, i.e., the sum of the internal energy ε and the kinetic energy per unit mass,

$$E = \varepsilon + \frac{1}{2}|\boldsymbol{v}|^2. \quad (19)$$

The rate of radiative energy loss per unit volume is given by Λn^2. The cooling function $\Lambda(T)$ used in FLASH is given by Rosner et al. (1978) in the temperature range $2 \times 10^4 \text{ K} < T < 10^8$ K, and by Peres et al. (1982) in the range $4 \times 10^3 \text{ K} < T < 2 \times 10^4$ K. We do not allow for radiative heating or heat conduction.

Throughout we also adopt an adiabatic equation of state, $P \propto \rho^\gamma$, where γ is the ratio of specific heats. In our simulations, we adopt $\gamma = 5/3$. Thus pressure and specific internal energy are related by $P = (\gamma - 1)\rho\varepsilon$. Finally, in all cases, we take the fluid to be a fully ionized proton-electron plasma, such that the density of the fluid is given by $\rho \approx m_p n_p$, with m_p being the proton mass and n_p the proton (and electron) number density. The electron contributions to pressure are significant and included; the electron contributions to density are small but nevertheless are also included. We do not allow for the possibility of recombination.

For the collision simulations, it is useful to be able to distinguish supernova material from that of the solar wind, and to measure the degree to which they mix. FLASH offers a convenient way to do this by introducing a new fluid variable C ("contamination"), which obeys

$$\frac{\partial (\rho C)}{\partial t} + \nabla \cdot (\rho C \boldsymbol{v}) = 0. \quad (20)$$

That is, the "mass scalar" C evolves passively, simply following the fluid element with which it was born. We inject supernova material with $C_{\rm SNR} = 1$ and solar wind material with $C_{\rm sw} = 0$; mixed material will thus have $0 < C < 1$. Thus a map of C over

the computational domain measures the penetration and mixing of supernova material.

Our simulations are thus aimed at addressing the basic hydrodynamics of the problem. We do not include magnetic fields, dust, or cosmic rays. As we will argue below (§ 8), these are unlikely to change the gross structure of the heliosphere in a collision with a supernova remnant. However, they may be crucial for a full quantitative understanding of the heliosphere in a collision with a supernova, and for the resulting geological signatures and astrobiology consequences of a nearby explosion. These will be the subject of future work.

5. SUPERNOVA REMNANT SIMULATIONS

5.1. *Supernova Remnant Model*

The simulations of the evolution of a supernova remnant served two purposes: (1) to test the accuracy of the code and (2) to provide the input parameters of pressure, density, and velocity of the shock impacting the heliosphere based on the distance of the explosion from the Sun. The model for the supernova explosion adopted for the simulation is that of an injection of energy into a small volume element. We neglect gravitational forces, heat conduction, and magnetic fields, but we allow for radiative cooling.

We impose axisymmetry, and thus set up a two-dimensional computational volume. To initialize the explosion, we inject an overpressure in a sphere centered at the origin and with a radius of no more than 1% of the extent of our computational domain, with an energy of $E_{\rm SN} = 10^{51}$ ergs. The rest of the computational domain is initialized with uniform density and pressure consistent with ISM parameters as listed in Table 1. The velocity of this ambient medium is zero in all directions.

5.2. *Supernova Remnant Evolution*

Our supernova simulations were done in axisymmetry (cylindrical coordinates), but for spherically symmetric initial conditions. Thus an immediate test of the code is its ability to maintain spherical symmetry throughout the system evolution. We indeed find that the remnant remains very accurately spherical. Consequently, we need not display the full two-dimensional results, but can instead summarize them completely in terms of the one-dimensional spherical properties.

Throughout the simulations the shock is very well resolved, reflecting the power of the FLASH shock-capturing algorithms. In Figure 1, we plot the shock position R as a function of time for explosions in media with two different densities. We see that in both cases, the shock trajectory displays the expected power-law behavior. In the lower density case corresponding to the Local Interstellar Cloud, the Sedov $R \sim t^{2/5}$ behavior is reproduced throughout, while in the high-density (average ISM) case, the initial Sedov behavior shows a transition to a $R \sim t^{1/4}$ trend.

The transition from an initial energy-conserving (Sedov) phase to a momentum-conserving (snowplow) phase occurs when energy losses become important. Radiative energy loss ("cooling") is mostly due to bremsstrahlung, and occurs at a rate per particle of $\Gamma_{\rm cool} \sim \Lambda n_e$. We expect significant energy losses when the cooling timescale $\tau_{\rm cool} = kT/\Gamma_{\rm cool}$ is on the order of the Sedov age $t_{\rm shock}$ (eq. [2]). Equating these gives an estimate for the transition to a radiative expansion at a distance of $R_{\rm rad} \simeq 30$ pc for $n_{p,\rm ISM} = 1$ cm^{-3}. Around this distance, one should see a change in the slope in $\log R - \log t$. A break in the slope is indeed seen in Figure 1, and occurs near 30 pc; this agreement adds to our confidence in our simulation, and will provide insight on the different hydrodynamic properties in the radiative phase.

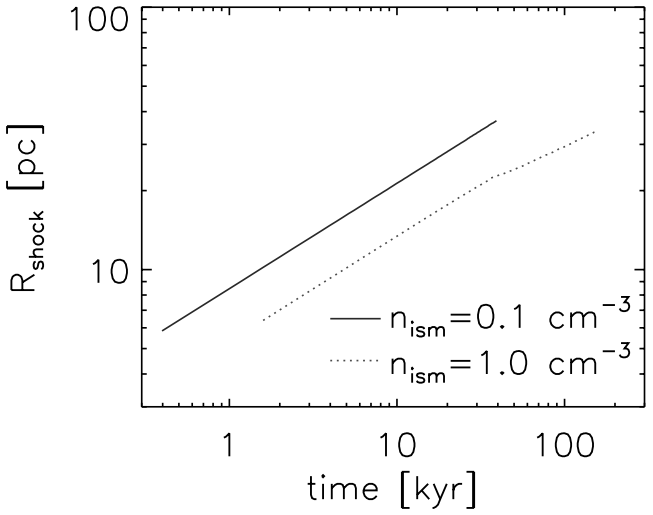

FIG. 1.—Shock trajectories for spherically symmetric supernova explosions in our two adopted ISM states (see Table 1). The shock position R follows the Sedov scaling $R \propto t^{2/5}$ for the entire low-density (Local Interstellar Cloud) simulation. In the high-density simulation, the initial Sedov (energy-conserving) phase ends when radiative energy losses become large, in this case at about $R \simeq 20$ pc. Thereafter, the SNR evolves in the snowplow phase, following the $R \propto t^{1/4}$ law from momentum conservation. [*See the electronic edition of the Journal for a color version of this figure.*]

The main results of the simulation are summarized in Table 2, which lists the postshock density, pressure, and velocity at distances of 10, 20, and 30 pc from the center of explosion. Results are given for the case where the supernova explodes in a $n_p = 0.1$ cm^{-3} and $T = 8000$ K medium like that of the Local Cloud today, and the case where it explodes in an ISM with $T = 8000$ K, but $n_p = 1$ cm^{-3} in order to investigate the effects of higher density and pressure, where the SNR can depart form the Sedov phase at large distances from the supernova. These results provide the input parameters for the supernova flow in the collision simulations.

Time profiles of the blast fluid properties are shown in Figure 2 for an observer located at a fixed distance $R = 10$ pc from the supernova explosion. Note that the time profile amounts to a sort of inversion of the blast profile in space. We see that the shock passage corresponds to the arrival of the densest, fastest, and highest pressure material, with these properties decaying with time as the slower, more rarefied, and hotter interior material passes the observer. We see that the density drop-off is fairly rapid compared to the supernova remnant age; still, the density remains within a factor of 2 of its peak value for $\gtrsim 1$ kyr in both cases. This verifies our expectations that a fixed observer sees the remnant properties change on timescales that are much larger than the dynamic timescales of the heliosphere itself. Thus in the context of our collision simulations, we are well justified in adopting the incident supernova blast properties as constant in space and time.

6. SOLAR WIND SIMULATIONS

6.1. *Solar Wind Model*

We simulate the solar wind as a spherically symmetric outflow. The solar wind simulation is over the same domain as the full collision simulation described below. The flow is spherically symmetric, but is solved in an axisymmetric domain, in cylindrical coordinates (r, z) with a spherical radius given by $R^2 = r^2 + z^2$. The $\pm z$ and $+r$ boundaries have outflow conditions imposed;

TABLE 2
SUPERNOVA BLAST PROPERTIES

DISTANCE, R_{SN} (pc)	DENSITY, $n_{p,SNR}$ (cm^{-3})	VELOCITY, v_{SNR} (km s^{-1})	PRESSURE (10^{-8} dyne cm^{-2})		ARRIVAL TIME, t_{cross} (kyr)	ADIABATIC EVOLUTION?
			$P_{SNR,ram}$	$P_{SNR,therm}$		
$E_{SN} = 10^{51}$ erg explosion into a $n_{p,ISM} = 0.005$ cm^{-3} medium (Local Bubble)						
10	0.02	8646	2.5	0.82	0.34	yes
20	0.02	3056	0.31	0.10	1.9	yes
30	0.02	1664	0.091	0.031	5.3	yes
$E_{SN} = 10^{51}$ erg explosion into a $n_{p,ISM} = 0.1$ cm^{-3} medium (Local Cloud)						
10	0.38	1940	2.4	0.82	1.5	yes
20	0.38	688	0.30	0.10	8.5	yes
30	0.39	375	0.091	0.031	23.4	yes
$E_{SN} = 10^{51}$ erg explosion into a $n_{p,ISM} = 1$ cm^{-3} medium						
10	3.8	614	2.4	0.82	4.8	yes
20	3.9	201	0.26	0.090	27	transition
30	31	131	0.0066	0.88	105	no

axisymmetry guarantees that there is no flow "across" $r = 0$, which is enforced by a reflecting boundary condition.

Because the length scales of interest to us ($\gtrsim$few $\times$ 0.1 AU) are much larger than the solar radius, in our simulation we inject the wind at a radius $R_{inj} \gg R_{\odot}$; the region interior to R_{inj} plays no role in our simulations. The fluid properties at injection are chosen to lead to solar wind behavior at 1 AU that is consistent with observations (§ 2.1). The rest of the computational volume in our solar wind simulations (and some collisions simulations) is initialized using the constant-velocity approximation above

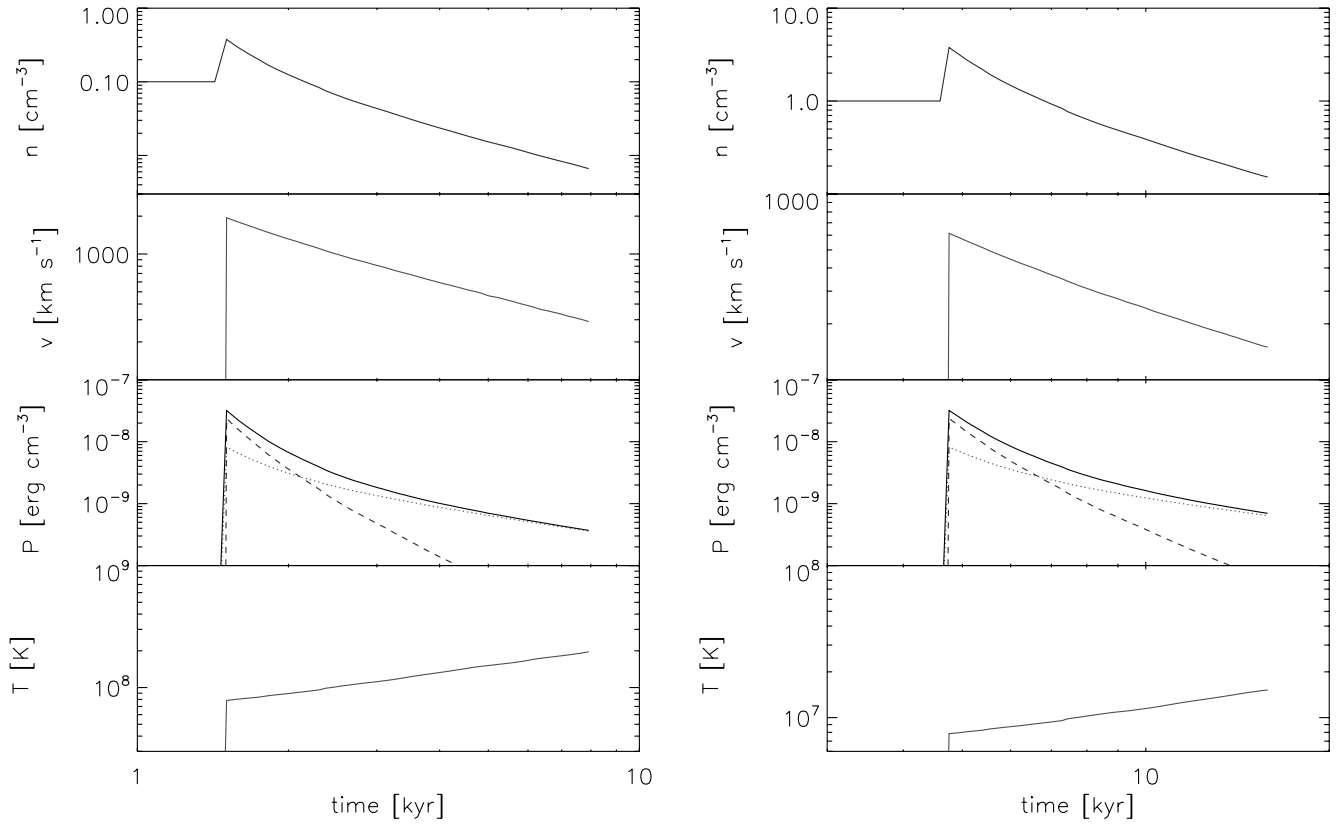

FIG. 2.—Time profiles of local fluid properties for an observer at a fixed distance $R = 10$ pc from a supernova blast of 10^{51} erg. The constant early time values are those of the ambient medium; the spike then denotes the arrival of the shock, which is followed by a drop in density and rise in temperature as the observer's location is engulfed in the SNR. The pressure curves display P_{therm} (*dotted lines*), P_{ram} (*dashed lines*), and $P_{tot} = P_{therm} + P_{ram}$ (*solid lines*). *Left*: Explosion into a Local Cloud medium. *Right*: Explosion into the average ISM. [*See the electronic edition of the Journal for a color version of this figure.*]

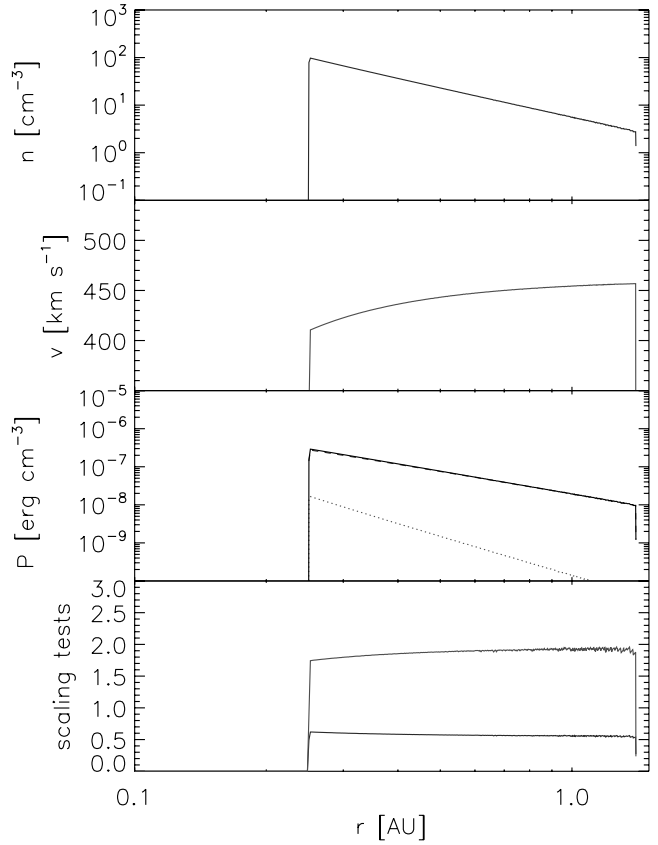

FIG. 3.—Radial profiles of solar wind fluid variables for a spherical, steady flow, which at $r = 1$ AU matches the average observed solar wind properties. The pressure curves display $P_{\rm therm}$ (*dotted line*), $P_{\rm ram}$ (*dashed line*), and $P_{\rm tot} = P_{\rm therm} + P_{\rm ram}$ (*solid line*). Note the restricted, linear scale for the velocity panel; the underlying message is that the velocity is nearly constant. In the bottom panel are plotted $r_{\rm AU}^2 n_p(r)/10$ cm^{-3} (*lower curve*) and $r_{\rm AU}^{2\gamma} P_{\rm ram}(r)/10^{-8}$ erg cm^{-3} (*upper curve*); note the linear scale. These test the scalings that would result if the velocity were perfectly constant: the curves would be exactly flat in that case. The nearly constant behavior of the curves confirms that the scalings (eqs. [12] and [13]) are excellent approximations to the full solution. [*See the electronic edition of the Journal for a color version of this figure.*]

(eqs. [11]–[13]). As seen in Figure 3, this approximation is very close to the full adiabatic solution, to which the domain adjusts itself within a few time steps.

We select the injection radius $R_{\rm inj}$ based on two considerations: (1) Small values of the injection radius introduce large asphericity in the flow when placed in the cylindrical coordinates of our grid; to minimize these asphericities imposes the computational expense of increasing the finest grid resolution. Thus computational speed and memory push for the largest possible injection radius. (2) On the other hand, the injection radius must lie safely away from the termination shock, particularly at its closest approach. As we will see, the termination shock and heliopause scale together, and are both set by pressure balance; thus we change the injection radius to follow the scales of the simulations. We find that a good compromise between these two competing demands is to initialize the solar wind at a radius in a range $R_{\rm inj} \sim 0.1$–0.5 AU, with the larger values corresponding to the larger overall computational domains; in general, this corresponds to about half of the termination shock's closest approach.

We include a point-mass gravitational source term, situated at the origin and having a mass $M_\odot$. In fact, gravitational effects are in practice small, because our injection radius is significantly beyond the sonic point, at which the wind becomes supersonic.

6.2. *Solar Wind Results*

The fluid evolves from an initial state set by the constant-velocity approximation above. Very rapidly the simulation relaxes to an adiabatic steady state. The relaxation timescale is, as one would anticipate, on the order of days per AU in radius (cf. eq. [15]). We find that the adiabatic solution has a velocity which is very nearly constant with radius; consequently the flow is very close to the "free wind" solution in which pressure and gravity forces are negligible. Thus, to a good approximation, we have a spatially constant velocity profile $v \approx v_{1\ \rm AU}$, and hence mass conservation demands $\rho(R_{\rm sw}) = \rho_{1\ \rm AU}(1\ {\rm AU}/R_{\rm sw})^2$. We see then that the analytic approximation we made in § 3.2 is a good one; in particular, the ram pressure scales as $P_{\rm ram} \propto R_{\rm sw}^{-2}$, as given in equation (13).

As with the supernova remnant simulations, we construct an axisymmetric grid to model a problem with spherical symmetry. Here again therefore, the degree of spherical symmetry in our results is a test of our code. We indeed find that the evolution maintains spherical symmetry quite well. Small asphericities necessarily do appear, manifesting as radial "spokes" in density and velocity maps. These numerical artifacts arise predominantly because of grid asphericities in the region at which the wind is injected. However, these asphericities are small: the density and velocity variations at a given spherical radius are always within $\lesssim$7% of the mean in the region of interest beyond $\gtrsim$0.5 AU.

7. SIMULATIONS OF SUPERNOVA COLLISION WITH THE SOLAR WIND

7.1. *Collision Model*

Having implemented prescriptions for the supernova and solar flows, we are now in a position to bring the two into collision. This simulation is of course the main goal of this paper. The basic structure of the simulation is a spherically symmetric outflow representing the solar wind, subject to an incident planar flow representing the supernova blast. The solar wind is injected as described in the previous section (§ 6.1). The supernova blast has the properties found for a particular time and distance in the simulations described in § 5.1. We examine the sensitivity of our results for different supernova distances and explosions into different media.

For computational expedience, we adopt a geometry that is axisymmetric about the stagnation line. The simulation thus is a grid in cylindrical coordinates (r, z), as in the solar wind simulations. The supernova flow is injected at the $-z$ boundary moving in the $+z$ direction; this makes z the symmetry axis, and thus the stagnation line is $r = 0$. The $+z$ and $+r$ boundaries have outflow conditions imposed.

The two-dimensional simulation can be performed fairly rapidly, so that we can explore the sensitivity of the winds to the parameters. Also, instabilities—notably Kelvin-Helmholtz—can and do develop in our simulations, and thus we are able to capture all of the most essential features of the hydrodynamic problem. Of course, the enforcement of axisymmetry does represent an important simplification. In particular, the instabilities in a full three-dimensional simulation may well be more substantial. Our work here will motivate further studies that will address these issues.

As noted in the discussion around equation (15), the natural timescale in our computational domain is on the order of days (down to hours for the crossing time over a single grid cell). Consequently, it is impracticable to model the entire $\gtrsim$1 kyr passage of the supernova blast. Indeed, we will find that this is not necessary, as the system will rapidly reach a quasi-static equilibrium.

TABLE 3
SIMULATION RESULTS: CHARACTERISTIC SCALES

Simulation Number	$\rho_{tot,sw}$ (1 AU) (10^{-24}g cm^{-3})	v_{sw}(1 AU) (km s^{-1})	R_{SN} (pc)	ρ_{SNR} (10^{-24} g cm^{-3})	v_{SNR} (km s^{-1})	r_{bal} (AU)	r_{ts} (AU)	r_{hp} (AU)
1.....	9.2	459	8	0.033	12084	0.62	0.62	0.87
2.....	9.6	455	10	0.033	8646	0.78	0.78	1.07
3.....	4.6	460	10	0.033	8646	0.54	0.55	0.80
4.....	4.8	459	10	0.059	4443	0.56	0.55	0.80
5.....	10.5	453	20	0.033	3057	2.29	2.11	3.34
6.....	5.0	456	8	0.63	2702	0.41	0.42	0.66
7.....	10.6	454	10	0.63	1940	0.83	0.82	1.20
8.....	4.8	459	10	0.63	1940	0.57	0.61	0.87
9.....	10.5	453	30	0.033	1664	4.21	4.41	5.88
10.....	9.6	468	10	1.1	1102	0.81	0.74	0.94
11.....	12.8	585	20	0.64	688	3.30	3.12	3.61
12.....	10.2	464	20	0.64	688	2.34	2.37	3.07
13.....	10.8	453	30	52	131	1.58	1.45	1.94
14.....	4.0	307	30	52	131	0.65	0.58	0.87
15.....	10.6	450	10	0.022	118	7.29	5.65	8.69

Also note that the simulation timescales are short enough that we do not need to average over the 11 yr solar cycle. In fact, we will investigate the effect of changes in the solar wind properties over the cycle.

We have examined two sets of initial conditions. One begins with the computational domain initialized as in the solar wind simulations. The supernova blast then enters the simulation and drives back the solar wind until a quasi–steady state heliosphere emerges. The other initialization fills the domain with the supernova flow into which the solar wind emerges, diverting the blast until a quasi–steady state again is reached. Because our problem has a quasi-steady solution, the results should be independent of the initial conditions once the simulation has relaxed to this state. We indeed find this to be the case.

7.2. *Collision Results*

We ran our simulations for a wide variety of SNR parameters and an observationally motivated set of variations in solar wind strengths. The input parameters and main quantitative outputs of these runs are summarized in Table 3. In this section, we will first focus on a few important cases that illustrate the general qualitative features of our simulations. Then we will turn to trends and scalings.

7.2.1. *Highlights from Individual Simulations*

We find that our simulations relax to a quasi–steady state in a timescale about equal to the supernova crossing time over the computational domain (eq. [15]). A still from such a relaxed simulation appears in Figure 4, model 7 in Table 3. This particular simulation corresponds to a supernova at 10 pc exploding into a Local Interstellar Cloud medium ($n = 0.1$ cm^{-3}) and colliding with a solar wind with the mean ram observed pressure (eq. [13]). However, the overall structure of the steady state supernova-compressed heliosphere is quite general, and obtains in all of the collision simulations we have run.

As seen in Figure 4, the basic structure is that of the present-day heliosphere for the case of a supersonic interstellar flow (e.g., Baranov 1990; Zank 1999). We see two shocks separated by a contact discontinuity. The supernova blast is decelerated in a bow shock, which we see has a characteristic smooth geometry and a shape and position that do not vary with time. The solar wind is similarly decelerated in a termination shock that surrounds the Sun. We see a forward/backward asymmetry in the termination shock. The termination shock has a time-invariant position and smooth shape in the "forward" region, i.e., where the solar wind velocity has a component in the $-z$-direction, and thus opposes the supernova blast. In the opposite "rearward" region, the termination shock has a more irregular geometry, which fluctuates

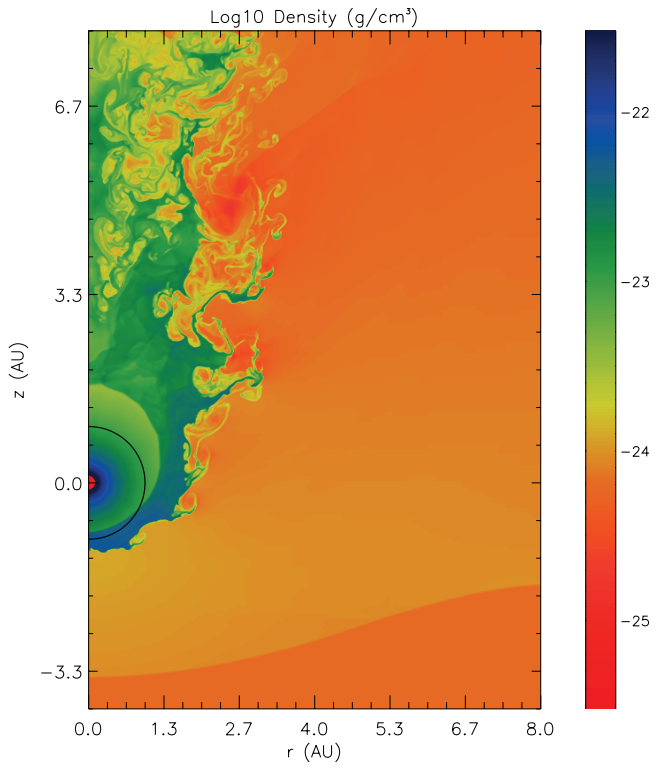

FIG. 4.—Snapshot of the heliosphere during the arrival of a shock from a supernova explosion 10 pc away, for model 7 in Table 3. The simulation uses cylindrical coordinates, with cylindrical r and z axes plotted; axisymmetry about the z axis is imposed. The Sun is located at the origin, and the SNR approaches from below; i.e., it advances in the $+z$-direction. The ambient ISM conditions are those of the present-day Local Interstellar Cloud. Plotted is a logarithmic density map. We see that two shocks develop: one surrounds the Sun and is due to the deceleration of the supersonic solar wind. The other is the bow shock due to the deceleration of the SNR. The flows then converge onto the heliopause, which can be seen as the ragged interface; the irregular shape is due to Kelvin-Helmholtz instabilities. A circle is drawn at a (spherical) radius of 1 AU, i.e., indicating the Earth's orbit (up to inclination effects). We see that a SNR under these conditions will penetrate to just beyond 1 AU.

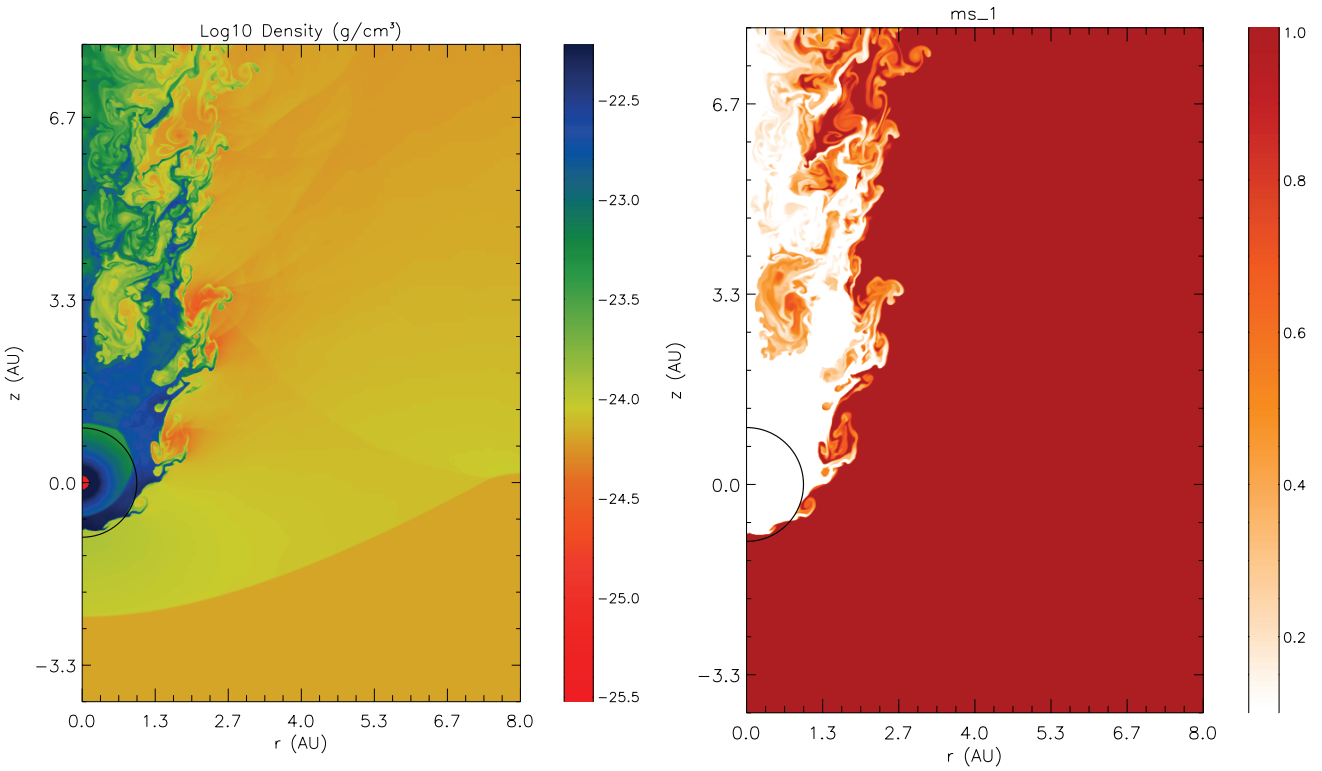

FIG. 5.—*Left*: Density map as in Fig. 4, for model 8 in Table 3. This is also for a supernova explosion at $R_{SN} = 10$ pc, but with a solar wind with a ram pressure set by $P_{ram,1AU} = 1.2 \times 10^{-8}$ dyne cm^{-2}. This is about half of the time-averaged mean observed value today (and used in Fig. 4), and also represents a 1 σ fluctuation below the mean. In this case, the supernova blast does engulf the Earth, and the Earth's orbit may carry it into the remnant where it will be directly exposed to supernova material. *Right*: Contamination map of the domain in the left panel; the $C = 1$ region corresponds to supernova material, the $C = 0$ region to solar material. We see that the supernova does penetrate to 1 AU, and also that in the disturbed flows rearward of the collision, the material becomes well mixed.

in time, as does the position of the shock. This is because the rearward shock arises because of the diversion of all of the radial solar outflow into highly disrupted flow moving in the $+z$ direction inside a small, roughly cylindrical region. We find that while this rearward termination shock is irregular in space and time, it is always more distant from the Sun than the forward shock.

Of particular interest to our problem is the contact discontinuity that develops between the two shocks. As with the solar wind, this heliopause marks the separation between the supernova and the solar material, and thus delimits the innermost boundary of the SNR. Figure 4 illustrates the general result that the heliopause has a structure that is highly irregular in space and time. These large fluctuations are due to Kelvin-Helmholtz instabilities caused by velocity shear at the interface between the two flows. Elongated structures in the instabilities can be sheared into large plumes of material ejected laterally into the supernova flow (i.e., in the $+r$-direction), further distorted as they are entrained in the blast, and finally carried out of the simulation domain. These instabilities are present at all polar angles from the Sun, up to the stagnation point. In particular, the forward region of closest supernova approach is subject to these instabilities, and the stagnation distance varies significantly over $\sim$1 day timescales, with fluctuations in distance often $\sim\pm$10% of the mean, and sometimes more.

Figure 4 not only illustrates the general structure of supernova–solar wind collisions, but also specifically the case of a 10 pc explosion (in a Local Interstellar Cloud medium, $n = 0.1$ cm^{-3}) onto an "average" solar wind. We see that the stagnation point, while somewhat variable, is located just barely beyond 1 AU. Several important conclusions follow from this result. First, we see that our full numerical simulations confirm (to within $\sim$10%) the simple pressure-balance stagnation estimate in equation (14). Also, taken at face value, the $\simeq$1.1 AU stagnation distance suggests that the *average* solar wind of the present epoch is just strong enough to prevent the Earth from being engulfed by a 10 pc supernova. However, as noted in § 3.3, the larger lesson to take from this result is that the question of supernova penetration to 1 AU is not an "open-and-shut case," but rather will be sensitive to the details of the problem. For example, we would expect a slightly closer (or more powerful) supernova, and/or a slightly weaker solar wind to lead to a successful supernova approach to within 1 AU.

To illustrate the sensitivity of the supernova penetration to the parameters in our problem, and to test the pressure-balance scalings, we show in Figure 5 the results from model 8 in Table 3. In this collision, the supernova properties are identical to those in Figure 4 (i.e., a 10 pc explosion into a Local Interstellar Cloud medium). However, the solar wind has a lower density, such that the ram pressure is $P_{ram,1\ AU} = 1.2 \times 10^{-8}$ dyne cm^{-2} at 1 AU. This value is about half that in Figure 4, and thus the solar wind ram pressure is correspondingly smaller throughout. This value corresponds to a fluctuation of slightly less than 1 σ below the time-averaged mean. In other words, this illustrates the heliosphere during a phase in which the solar wind is slightly weakened to a level still quite commonly observed. We see that in this case, the supernova now does penetrate to just within 1 AU, and thus the Earth can be directly exposed to remnant material. This point is made clear in Figure 5*b*, which shows the "contamination" mass scalar field (eq. [20]); we also see that in the flow trailing the rearward termination shock, supernova and solar wind material is interspersed in complex eddies, and is often well mixed.

To show the effect of the supernova blast, we plot in Figure 6 the results for a more distant supernova, model 12 in Table 3. The

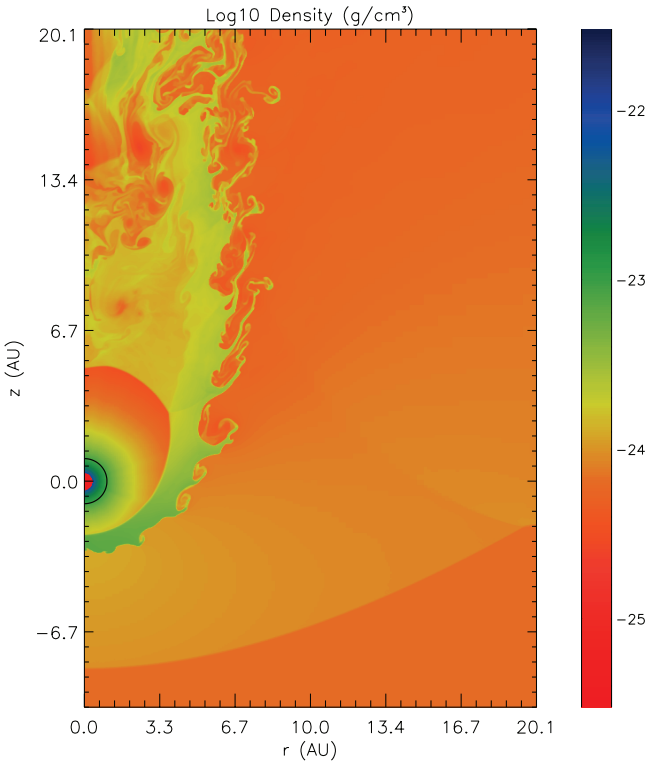

FIG. 6.—Same as Fig. 4, but for a supernova at $R_{SN} = 20$ pc; this is model 12 in Table 3. Note the enlarged scale. We see a similar overall structure, but the heliopause has now moved well beyond 1 AU. In this case, the supernova blast would not engulf the Earth.

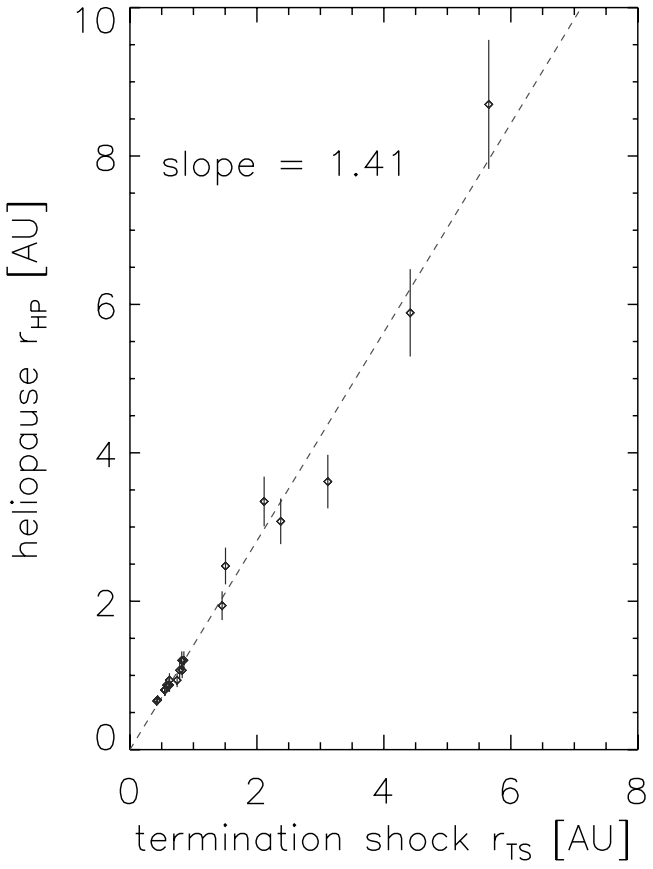

FIG. 7.—Plot of the innermost approach of the heliopause (r_{hp}) vs. that of the termination shock (r_{ts}) for the solar wind–supernova collision models we have run. Error flags on the heliopause reflect the ~10% fluctuations that arise due to Kelvin-Helmholtz instabilities. A very strong linear correlation is observed, with an intercept consistent with zero. A linear relation $r_{hp} = 1.41 r_{ts}$ provides the best fit to all the data, for a wide range in supernova distance and in the relative contribution from supernova thermal vs. ram pressure. The universality of this scaling shows that pressure balance is the controlling factor for the collision geometry and scalings. [*See the electronic edition of the Journal for a color version of this figure.*]

blast parameters are those of an explosion at 20 pc, with a Local Interstellar Cloud ambient medium (Table 2). The solar wind is restored to its full-strength, time-averaged mean observed value. Noting the change in scale in the plot, we see that the supernova penetrates to the inner solar system, but that now the stagnation radius, at about 3 AU, is far from Earth.

7.2.2. *Scaling Relations from the Full Suite of Simulations*

We have performed a suite of other simulations, spanning a wide variety of supernova distances and a range of solar wind parameters reflecting the observed time variations in wind properties. This parameter study and our analysis of its results applies the approach of Müller et al. (2006) to our case of a supernova-confined heliosphere. Input parameters and resulting locations of the termination shock r_{ts} and heliopause r_{hp} appear in Table 3. Also tabulated is the pressure-balance distance r_{bal}, computed using equation (14), the solar wind, and supernova properties.

These data are well described by simple scaling relations, as expected based on the analytical arguments above, and in agreement with other studies of the heliosphere under less drastic conditions. Figure 7 displays the tight correlation between the locations of the termination shock and the heliopause at their closest approach (i.e., along the $-z$ symmetry axis). Error bars in the vertical axis reflect the ~10% fluctuations in the heliopause location due to instabilities. A linear relation is clearly evident, and a least-squares fit gives an intercept consistent with zero and a slope of $r_{hp}/r_{ts} = 1.4$.

This result is interesting for several reasons. First, from a purely empirical point of view, it is remarkable that such a simple relationship accurately summarizes the behavior of a wide variety of flows (supernova dynamic pressures spanning 2 orders of magnitude). This empirical relationship is also useful for the supernova problem, as it allows for determination of both of these heliospheric dimensions if either of the two boundaries can be predicted. Also, the specific slope of 1.4 is intriguing because this is precisely the value obtained for the same slope in the Müller et al. (2006) simulations. That the agreement is so close is nontrivial and perhaps even surprising, given their significantly slower interstellar flow and, more importantly, the inclusion of neutral species in their multifluid results. A naïve interpretation of the similarity between our result and that of Müller et al. (2006) would be that this scaling arises from the basic hydrodynamics, and is not strongly sensitive to multifluid effects. However, a full exploration of this comparison must await the inclusion of neutrals in our simulations.

The simplicity and robustness of the scaling between termination shock and heliopause suggests that the gross characteristics of our results are the result of an equilibrium, such as the momentum balance between pressure forces. Using our suite of models, we can compare the pressure-balance distance r_{bal} (eq. [14]) to the characteristic scales observed in the simulations. Since we have seen that the termination shock and heliopause location scale in a linear way, comparison of r_{bal} with either will suffice for both.

In the top panel of Figure 8, we plot r_{bal} versus the termination shock location for our simulations. We again see a tight correlation, now with a slope very close to unity. We thus find that the simple pressure-balance distance as given in equation (14) turns out to

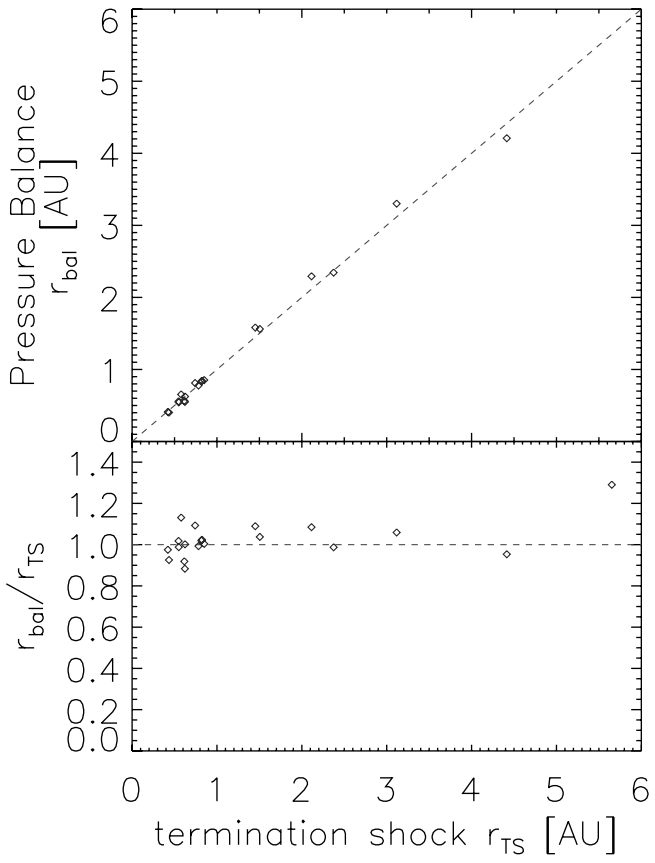

FIG. 8.—Illustration of the success of pressure balance in accounting for the heliospheric structure. The distance $r_{\rm bal}$ for solar wind–supernova pressure balance is computed as in eq. (14) for each simulation. Results are plotted as a function of termination shock distance $r_{\rm ts}$; the dotted line is for $r_{\rm bal} = r_{\rm ts}$, i.e., with a slope of 1. *Top*: Plot of $r_{\rm bal}$ vs. $r_{\rm ts}$, showing a tight correlation. *Bottom*: The small ~10%–20% scatter in the ratio $r_{\rm bal}/r_{\rm ts}$ quantifies the accuracy of the pressure balance scaling. [*See the electronic edition of the Journal for a color version of this figure.*]

be an excellent predictor of the termination shock location. The accuracy of this prediction can be seen in the bottom panel of Figure 8, which shows the residual of the scaling, i.e., the scatter in the ratio $r_{\rm bal}/r_{\rm ts}$. We see that the scaling always holds to within 20%, and often to better than 10%.

It is of interest that the pressure-balance distance predicts the location of the termination shock, rather than the heliopause, which our simulations show to lie a factor of 1.4 beyond. For practical purposes, we can combine these two scalings to infer the heliopause position as

$$r_{\rm hp} = 1.4 r_{\rm bal}. \tag{21}$$

This can be used to estimate the heliopause position as a function of distance from a supernova whose remnant is in the Sedov phase. Furthermore, the sensitivity to supernova distance is

$$r_{\rm hp} = 1.2 \text{ AU} \left(\frac{P_{\rm sw} + \rho_{\rm sw} v_{\rm sw}^2}{2 \times 10^{-8} \text{ dyne cm}^{-2}}\right)^{1/2} \left(\frac{R_{\rm SN}}{10 \text{ pc}}\right)^{3/2}, \tag{22}$$

and thus we see that to penetrate within $r_{\rm hp} \leq 1$ AU, under typical solar wind conditions, requires a supernova within $R_{\rm SN} \leq 9$ pc.

These empirical results vindicate and encourage the use of the simple estimates and scalings for the collision properties presented in § 3.3. Given the other uncertainties and complexities of the problem, we find the usefulness of these scalings to be heartening, allowing one to focus attention on the most relevant parts of parameter space.

8. DISCUSSION

The Knie et al. (1999, 2004) detection and confirmation of live ^{60}Fe in a ~2–3 Myr old sedimentary layer stands as the first evidence for the terrestrial deposition of debris from a recent nearby supernova. To qualitatively and quantitatively understand and interpret these provocative data requires a reliable accounting of the penetration of supernova ejecta into the solar system. To this end, we have performed the first hydrodynamic simulation of the collision between a supernova blast and the solar wind, using the FLASH code (Fryxell et al. 2000).

To study the supernova impact, we first made a simple spherically symmetric hydrodynamic model of a supernova remnant with cooling; this provided the time profile of blast properties at various distances from the explosion. We used these results in our main, two-dimensional simulations, in which the heliosphere is described by a spherically symmetric solar wind, subject to an incident planar wind with the properties of a supernova blast at a selected distance. We found that the resulting heliosphere displays a morphology qualitatively similar to the results of theoretical and numerical studies of the heliosphere under present-day conditions (Zank 1999). The deceleration of the supersonic solar and supernova flows leads to a termination shock and a bow shock. These shocks are separated by a contact discontinuity that marks the boundary between supernova ejecta and solar material.

We further see that our results display a linear scaling between termination shock and heliopause location that is in excellent quantitative agreement with the extensive Müller et al. (2006) simulations of the heliosphere under a wide variety of conditions. Our work builds on their results and extends them to the supernova regime with dynamic pressures an order of magnitude higher. It is important to note that the multifluid simulations of Müller et al. (2006) include the effects of interstellar neutrals, which are important both for the present heliosphere and the perturbed environments they consider. In our supernova case, the extreme temperatures of young remnants will not allow for neutrals. On the other hand, older supernova remnants could contain high-density regions with a nonzero neutral fraction; these might show interesting effects which bear further future study.

The strength of the supernova blast far exceeds that of the relative interstellar wind seen today by the Sun, and so quantitatively, the heliospheric boundaries in our simulations are pushed far closer than those observed today. In particular, the closest approach of the supernova material extends almost exactly to 1 AU for an explosion at 10 pc, and to within a few AU for an explosion at 20 pc; we find that simple scaling laws based on a pressure-balance argument (Baranov 1990) provide a surprisingly accurate and useful description of the behavior of this stagnation point. We also find that mixing between the supernova and solar wind material occurs only in a thin region on either side of the contact discontinuity on the front side of the collision; consequently, the discontinuity itself provides a good measure of the innermost boundary for penetration of SNR material. On the other hand, the material trailing the heliopause has intertwined pockets of material ranging from purely supernova, to purely solar, to well mixed.

Our results have implications for the 2.8 Myr old ^{60}Fe signal of Knie et al. (1999, 2004) and for nearby supernova debris deposition generally. We find that the maximum supernova penetration distance exceeds 1 AU for explosions beyond 10–20 pc from the Sun. Thus, our models would indicate that the Earth is never engulfed within the supernova remnant for most distant explosions.

Of course, the precise quantitative "cutoff" distance for terrestrial exposure will depend on the details of the problem, some of which we have simplified (notably, we have performed a 2D calculation, with no magnetic fields). Nevertheless, we suspect that these effects will not strongly alter the cutoff, and thus direct terrestrial deposition of supernova ejecta may indeed not occur for events beyond $\sim$20 pc. On the other hand, the ^{60}Fe abundance points to a distance range of 10–100 pc (Fields et al. 2005). Thus we would conclude that the supernova event leading to the ^{60}Fe signal either must lie at or near the lower distance limit (pointing to a low ^{60}Fe nucleosynthesis yield), or that the ^{60}Fe deposition did not require that the supernova remnant penetrate all the way to 1 AU.[4]

How could radioisotope deposition occur for supernovae whose blasts do not penetrate to the Earth? A possible mechanism suggests itself on considering that most heavy elements produced in supernovae, including all of those with long-lived radioisotopes, are refractory and condense rapidly from the gas phase onto dust grains. These particles are far less affected by the solar wind than the supernova plasma, and we suspect that dust penetrates the solar system much more readily and is deposited terrestrially. Indeed, even today, interstellar grains penetrate to 1 AU while moving at speeds an order of magnitude slower than grains entrained in a supernova blast would be. Thus, the penetration of the supernova remnant itself could deliver dust grains to the inner solar system, where they would then follow their own trajectories into the heliosphere and to the Earth. This possibility will be examined in detail in a forthcoming study.[5]

Our results also have implications for astrobiology. The "kill radius" of a supernova is estimated to be $\sim$8 pc (Ellis & Schramm 1995; Gehrels et al. 2003). We have found that a supernova blast launched from such a short distance can penetrate to within 1 AU. This implies that biologically damaging events will indeed be accompanied by radioisotope deposition. We conclude therefore that a nearby supernova capable of leading to a paleontological extinction signal will be accompanied by a radioisotopic signal. Thus the presence and severity of supernova damage can be independently corroborated and calibrated. Not only does this allow one to confirm a supernova as the source of an extinction event, but this also differentiates supernova damage from the very similar environmental and biological effects of a Galactic gamma-ray burst (Melott et al. 2004; Thomas et al. 2005; Scalo & Wheeler 2002).

As we have emphasized, our study represents the first model for a supernova impact on the heliosphere, and we have therefore intentionally adopted some simplifying assumptions. In future work, we will extend the present results by refining our treatment of the physics and astrophysics of the problem. Future hydrodynamic calculations will investigate the effect of magnetic fields in the solar wind and in the SNR. We also intend to remove the assumption of axisymmetry to examine the role of Kelvin-Helmholtz instabilities both with and without magnetic fields. In addition, as noted above, we plan to address the issue of supernova dust penetration of the solar system. Our results here provide motivation and lay the foundations for these studies.

[4] Even supernovae that do not reach 1 AU, but still compress the heliopause within $\sim$5 AU, will directly deposit supernova debris in the asteroid belt, which can later be transported to Earth as meteoritic material. If such material could be detected, it would open the supernova direct deposit distance range considerably, in some cases extending to explosions at 30 pc (cf. Table 3). We thank the anonymous referee for pointing this out.

[5] Neutral atoms and/or dust grains also can penetrate the heliosphere with some efficiency (Zank 1999 and references therein). Yeghikyan & Fahr (2004) note that infalling neutral hydrogen can lead to water formation in the Earth's upper atmosphere, at the expense of ozone; they suggest that a sufficiently high H I flux ($\gtrsim 10^9$ atoms cm^{-2} s^{-1}) could lead to significant depletion of atmospheric ozone. This effect would be an additional source of supernova ozone damage beyond that due to ionizing radiation (e.g., Ruderman 1974; Gehrels et al. 2003).

We are pleased to acknowledge helpful discussions with Günther Korschinek, Klaus Knie, Adrian Melott, Michael Paul, John Scalo, Alex Heger, Priscilla Frisch, and You-Hua Chu. We are grateful to Ghazi Zouaoui for assistance in the early stages of this work. We are particularly indebted to Paul Ricker for enlightening conversations and for invaluable assistance with the FLASH code, and to the anonymous referee, whose suggestions greatly improved the paper. The software used in this work was in part developed by the DOE-supported ASC/Alliance Center for Astrophysical Thermonuclear Flashes at the University of Chicago. This work was supported by NASA Exobiology grant EXB03–0000-0031.

REFERENCES

Axford, W. I., Dessler, A. J., & Gottlieb, B. 1963, ApJ, 137, 1268
Baranov, V. B. 1990, Space Sci. Rev., 52, 89
Basu, S., Stuart, F. M., Schnabel, C., & Klemm, V. 2007, Phys. Rev. Lett., 98, 141103
Benítez, N., Maíz-Apellániz, J., & Canelles, M. 2002, Phys. Rev. Lett., 88, 81101
Burlaga, L. F., Ness, N. F., Acuña, M. H., Lepping, R. P., Connerney, J. E. P., Stone, E. C., & McDonald, F. B. 2005, Science, 309, 2027
Crutzen, P. J., & Brühl, C. 1996, Proc. Natl. Acad. Sci., 93, 1582
Ellis, J., Fields, B. D., & Schramm, D. N. 1996, ApJ, 470, 1227
Ellis, J., & Schramm, D. N. 1995, Proc. Natl. Acad. Sci., 92, 235
Fields, B. D. 2004, NewA Rev., 48, 119
Fields, B. D., & Ellis, J. 1999, NewA, 4, 419
Fields, B. D., Hochmuth, K. A., & Ellis, J. 2005, ApJ, 621, 902
Florinski, V., Zank, G. P., & Pogorelov, N. V. 2005, Adv. Space Res., 35, 2061
Frisch, P. C. 1995, Space Sci. Rev., 72, 499
Fryxell, B., et al. 2000, ApJS, 131, 273
Gehrels, N., Laird, C. M., Jackman, C. H., Cannizzo, J. K., Mattson, B. J., & Chen, W. 2003, ApJ, 585, 1169
Ipavich, F. M., et al. 1998, J. Geophys. Res., 103, 17205
Karam, P. A. 2002a, Radiat. Phys. Chem., 64, 77
———. 2002b, Health Physics, 82, 491
Knie, K., Korschinek, G., Faestermann, T., Dorfi, E. A., Rugel, G., & Wallner, A. 2004, Phys. Rev. Lett., 93, 171103
Knie, K., Korschinek, G., Faestermann, T., Wallner, C., Scholten, J., & Hillebrandt, W. 1999, Phys. Rev. Lett., 83, 18
Krasovskii, V. I., & Shklovskii, I. S. 1957, Akad. Nauk SSSR Dokl., 116, 197
Krimigis, S. M., Decker, R. B., Hill, M. E., Armstrong, T. P., Gloeckler, G., Hamilton, D. C., Lanzerotti, L. J., & Roelof, E. C. 2003, Nature, 426, 45
Kryukov, I. A., Borovikov, S. N., Pogorelov, N. V., & Zank, G. P. 2006, in AIP Conf. Proc. 858, Physics of the Inner Heliosheath: Voyager Observations, Theory, and Future Prospects, ed. J. Heerikhuisen (New York: AIP), 39
Landau, L. D., & Lifshitz, E. M. 1987, Fluid Mechanics, 2nd ed. (Oxford: Pergamon Press)
Laster, H., Tucker, W. H., & Terry, K. D. 1968, Science, 160, 1138
Leinert, C., & Jackson, B. V. 1998, ApJ, 505, 984
Luo, D., McCray, R., & Mac Low, M. 1990, ApJ, 362, 267
McDonald, F. B., Stone, E. C., Cummings, A. C., Heikkila, B., Lal, N., & Webber, W. R. 2003, Nature, 426, 48
Melott, A. L., et al. 2004, Int. J. Astrobiology, 3, 55
Mullan, D. J. 1983, ApJ, 272, 325
Müller, H.-R., Frisch, P. C., Florinski, V., & Zank, G. P. 2006, ApJ, 647, 1491
Patterson, T. N. L., Johnson, F. S., & Hanson, W. B. 1963, Planet. Space Sci., 11, 767
Peres, G., Serio, S., Vaiana, G. S., & Rosner, R. 1982, ApJ, 252, 791
Phillips, J. L., et al. 1995, Geophys. Res. Lett., 22, 3301
Rosner, R., Tucker, W. H., & Vaiana, G. S. 1978, ApJ, 220, 643
Ruderman, M. A. 1974, Science, 184, 1079

Scalo, J., & Wheeler, J. C. 2002, ApJ, 566, 723
Schindewolf, O. H. 1954, Neues Jahrbuch für Geologie und Paleontäontologie Monatshefte, 10, 457
Shklovskii I. S. 1968, Supernovae (New York: Wiley)
Smith, R. K., & Cox, D. P. 2001, ApJS, 134, 283
Steinitz, R., & Eyni, M. 1980, ApJ, 241, 417
Stevens, I. R., Blondin, J. M., & Pollock, A. M. T. 1992, ApJ, 386, 265
Stone, E. C., Cummings, A. C., McDonald, F. B., Heikkila, B. C., Lal, N., & Webber, W. R. 2005, Science, 309, 2017
Terry, K. D., & Tucker, W. H. 1968, Science, 159, 421
Thomas, B. C., et al. 2005, ApJ, 634, 509
Velázquez, P. F., Koenigsberger, G., & Raga, A. C. 2003, ApJ, 584, 284
Webber, W. R. 2005, J. Geophys. Res. Space Phys., 110, 10103
Woodward, P., & Colella, P. 1984, J. Comput. Phys., 54, 115
Yeghikyan, A., & Fahr, H. 2004, A&A, 425, 1113
Zank, G. P. 1999, Space Sci. Rev., 89, 413
Zank, G. P., & Frisch, P. C. 1999, ApJ, 518, 965